

Formation of Dense Partonic Matter in High Energy Heavy-Ion Collisions: Highlights of RHIC Results

Rachid Nouicer

Brookhaven National Laboratory, Physics Department, Building 510D
Upton, New York 11973-5000, U.S.A.

Received: date / Revised version: date

Abstract. I review some important results from RHIC experiments. They were obtained in a unique environment for studying QCD bulk matter at temperatures and densities that surpass the limits where hadrons can exist as individual entities, raising the quark-gluon degrees of freedom to prominence. These findings support the major experimental observations from measuring the bulk properties of particle production, particle ratios and chemical freeze-out conditions, elliptic flow followed by hard probes measurements: di-jet fragment azimuthal correlations, high- p_T hadron suppression, and heavy-flavors probes. I present the measurements as a function of collision centrality, energy, system size and for different particle species. These results reveal that a dense strongly interacting medium was created in central Au + Au collisions at $\sqrt{s_{NN}} = 200$ GeV: the RHIC discovery. Further, they suggest that this medium is partonic. However, the discoveries so far observed at RHIC are far from being understood fully. Accordingly, the focus of the experiments has shifted from the discovery phase to the detailed exploration phase of the properties of this medium.

PACS. 25.75.-q – Relativistic heavy-ion collisions, 25.75.Ag – Global features, 25.75.Ld – Collective flow, 25.75.Gz – Particle correlations, 25.75.Bh – Hard scattering, 25.75.Cj – Heavy quark production, 25.75.Nq – Quark-gluon plasma production

1 Physics motivation and RHIC achievements

Quantum Chromodynamics (QCD) is considered the fundamental theory for strong interactions. According to it, hadronic matter under extreme dense and hot conditions must undergo a phase transition [1] to form a Quark Gluon Plasma (QGP) in which quarks and gluons no longer are confined to the size of a hadron. Recent results from lattice QCD at finite temperature [2,3] reveal a rapid increase in the number of degrees of freedom associated with this deconfinement of quarks and gluons from the hadronic chains. The transition point is at a temperature $T \approx 170$ MeV and energy density $\epsilon \approx 1$ GeV/fm³. Under the same conditions, chiral symmetry is restored [2]. Therefore, experiments search for signatures of both QGP formation and the in-medium effects of hadron properties. It was proposed that the required high densities could be achieved via relativistic heavy ion collisions [4].

Under RHIC (Relativistic Heavy Ion Collider) project, an accelerator was constructed at Brookhaven National Laboratory (BNL) from 1991 to 1999. RHIC was designed as a heavy-ion machine, able to support the collision of a wide range of nuclei over a large range of energies. Already, gold-gold, copper-copper and deuteron-gold collisions have been attained at energies from $\sqrt{s_{NN}} = 19.6$

to 200 GeV. Further, a polarized capability was added to RHIC allowing transverse and longitudinal polarized protons to collide at energies from $\sqrt{s_{NN}} = 200$ to 410 GeV. By now, RHIC has made a major physics discovery, namely the creation in high-energy central gold-gold collisions of a new form of matter; dense and strongly interacting, called the strongly coupled quark-gluon plasma, or sQGP. This finding was rated the top physics story of 2005 and the four experiments at RHIC, BRAHMS, PHENIX, PHOBOS, and STAR, published, in white papers, evidence of the existence of this new form of matter [6]. RHIC accelerator also met and surpassed its specifications; namely, it attained its energy goals, and exceeded the heavy-ion luminosity goals by factor of 2, and polarized proton luminosity by a factor of 5. Table 1 summarized the achievements of RHIC over the last eight years.

In this article, I highlight the recent RHIC results underlying the major experimental observations, i.e., “discoveries”. I start with discussions of bulk particle production and the initial conditions, followed by particle ratios and chemical freeze-out conditions. I then present our measurements of elliptic flow that are an indirect signature of the existence of partonic matter, followed by hard-probe measurements: di-jet fragment azimuthal correlations, high- p_T hadron suppression, and heavy-flavors probes. These measurements of hard probes afford direct

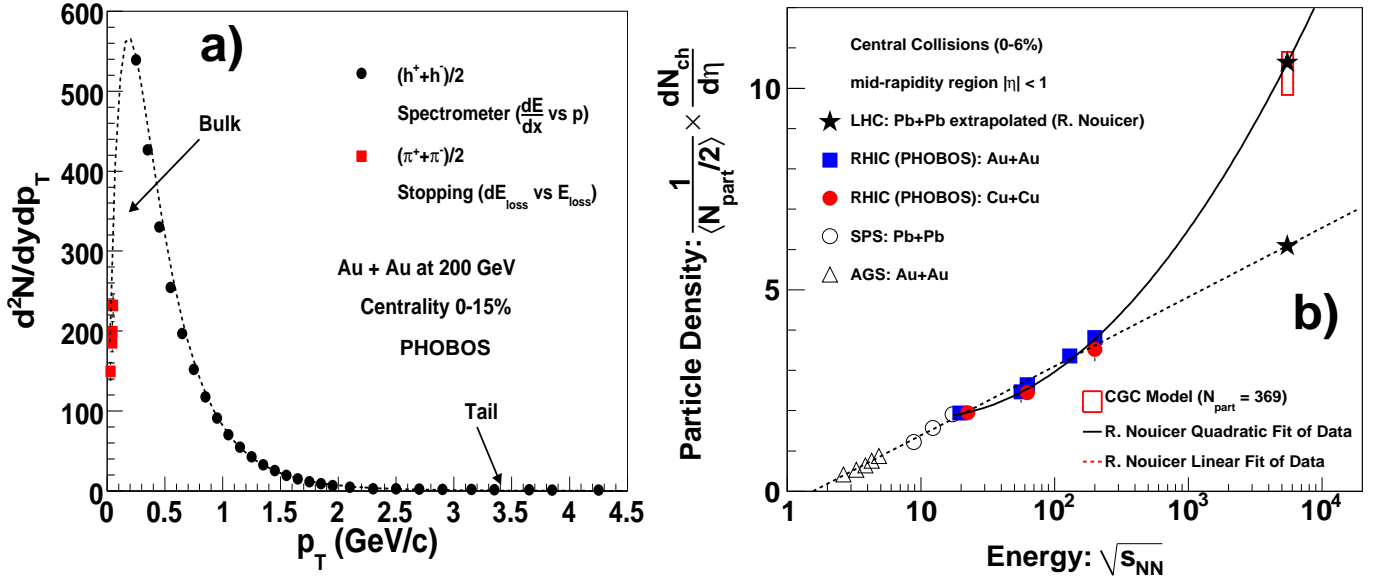


Fig. 1. Panel a) The measured distribution of charged-hadron as a function of transverse momentum p_T for the 15% most central Au + Au collisions at $\sqrt{s_{NN}} = 200$ GeV. Panel b) The measured scaled pseudorapidity density $dN_{ch}/d\eta/\langle \frac{1}{2}N_{part} \rangle$ for $|\eta| < 1$ in central Au+Au collisions at the AGS, in central Au + Au and Cu + Cu collisions at the RHIC and in central Pb + Pb collisions at the SPS [8,9,10,11]. The star symbols denote the extrapolation for $dN_{ch}/d\eta/\langle \frac{1}{2}N_{part} \rangle$ in central Pb + Pb collisions at 5.5 TeV (LHC). The continuous curve corresponds to the logarithmic quadratic fit of the RHIC data: $f_{AA}^Q = 3.09 - 1.06\ln(\sqrt{s_{NN}}) + 0.22(\ln(\sqrt{s_{NN}}))^2$. The dashed line represents the logarithmic linear fit of the AGS, SPS and RHIC data: $f_{AA}^L = 0.4749 + 0.77 \ln(\sqrt{s_{NN}})$. The error bars show the systematic errors. The Color Glass Condensate model (CGC model) prediction for LHC is also illustrated as a red box [12].

signatures of highly interacting dense matter created in central Au + Au collisions at $\sqrt{s_{NN}} = 200$ GeV. The measurements, for different particle species, are given as a function of collision centrality, energy, and system sizes.

2 Global properties of hadron production

Measurements of charged-particle multiplicity and transverse energy distributions, and of azimuthal anisotropies in heavy-ion collisions afford information on the initial energy density and the entropy production during the system’s evolution, and are sensitive to a variety of physics processes responsible for generating multiparticles. This knowledge is important for constraining model predictions and indispensable for understanding and estimating the accuracy of the more detailed measurements of, for example, jet or quarkonia production. Figure 1a shows the measured distribution of charged-hadrons produced in the 15% most central Au + Au collisions at $\sqrt{s_{NN}} = 200$ GeV [7]. The distribution illustrates a “bulk” and “tail” that are respectively related to “soft” and “hard” parton-parton scattering. We clearly observed that the “bulk” constitutes the dominant part of charged-hadron production. However, there is no clear separation between “soft” and “hard” processes. For this reason, an analysis undertaken as a function of centrality, transverse momentum, energy, and system sizes is required for better understanding particle production.

2.1 Charged-particle density distributions and initial conditions

One important observable in heavy-ion interactions is the number of charged-particles produced in a collision, called the charged-particle pseudorapidity density $dN_{ch}/d\eta$. This number ($dN_{ch}/d\eta$) is proportional to the entropy density at freeze-out and, since entropy cannot be destroyed (even in non-equilibrium systems), pseudorapidity density provides information on the initial state of parton density, and any further entropy produced during subsequent evolution [8].

Fig. 1b shows the charged particle densities near the mid-rapidity region, $dN_{ch}/d\eta|_{|\eta| < 1}/\langle N_{part}/2 \rangle$, where $\langle N_{part} \rangle$ is the average number of nucleon participant pairs, for Au + Au (RHIC: 19.6, 62.4, 130 and 200 GeV), Cu + Cu (RHIC: 22.4, 62.4 and 200 GeV), Pb + Pb (SPS: 8.83, 12.28 and 17.26 GeV) and Au + Au (AGS: 2.63, 3.28, 3.84, 4.29, 4.86 GeV); they present the 6% most central collisions as a function of center-of-mass collision energy ($\sqrt{s_{NN}}$) [8,9,10,11]. The results in this figure (see Fig. 1b) suggest that the particle density rises approximately logarithmically with energy. Comparing the finding for Cu + Cu and Au + Au indicates that, for the most central events in symmetric nucleus-nucleus collisions, the particle density per nucleon participant-pair does not depend on the size of the two colliding nuclei but only on the collision’s energy [10,11].

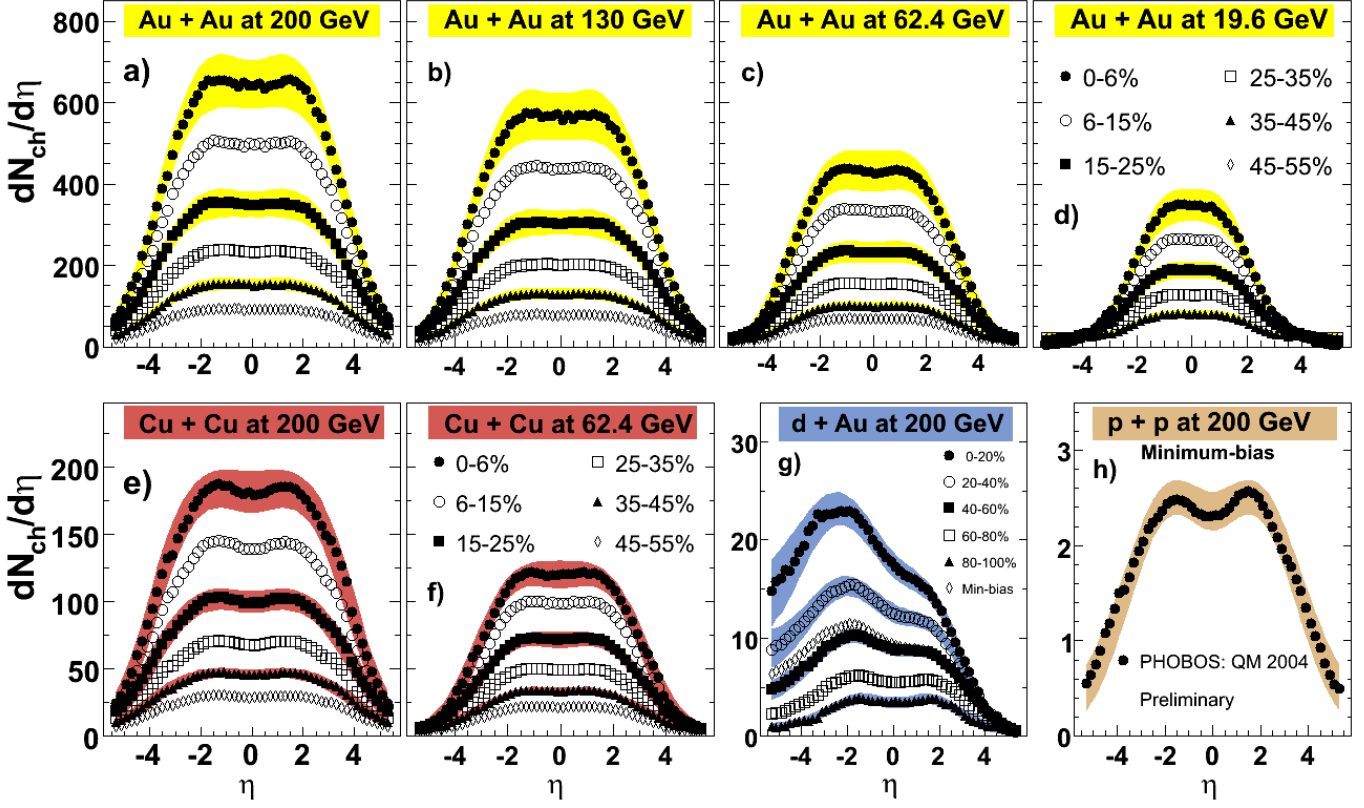


Fig. 2. The measured distributions of pseudorapidity density in Au + Au, Cu + Cu, d + Au, and p + p collisions at RHIC energies [8,9,10,11]. The $dN_{ch}/d\eta$ distributions for Au + Au, Cu + Cu and d + Au collisions are plotted as a function of collision centrality. Typical systematic errors (90% C.L.) are represented as bands for selected centrality bins. Statistical errors are negligible.

Based on the data presented in the Fig. 1b, we can establish two types of fits to predict (extrapolate) the results of $dN_{ch}/d\eta$ at the mid-rapidity region in Pb + Pb collisions at the LHC energy 5.5 TeV:

1. The logarithmic quadratic fit of the RHIC data is shown as the solid curve in Fig. 1b and its fit function is:

$$f_{AA}^Q = 3.11 - 1.07 \ln(\sqrt{s_{NN}}) + 0.23 (\ln(\sqrt{s_{NN}}))^2 \quad (1)$$

this formulation allows us to extrapolate the scaled density per nucleon participant pair for central Pb + Pb collisions at LHC energy (5.5 TeV):

$$\frac{1}{\langle N_{part}/2 \rangle} \times \frac{dN_{ch}}{d\eta}(\text{Pb} + \text{Pb at 5.5 TeV}) = 10.95$$

Using a Glauber model calculation for the 6% most central Pb + Pb collisions at 5.5 TeV (the total inelastic cross section used in the Glauber model calculation is $\sigma_{NN} = 64$ mb), we obtained the value of $\langle N_{part} \rangle = 365.5$, from which we can deduce the value of the unscaled pseudorapidity density at the mid-rapidity region:

$$\frac{dN_{ch}}{d\eta}(\text{central : 0 - 6\%, Pb} + \text{Pb at 5.5 TeV}) = 2002$$

2. The logarithmic linear fit of the data from the AGS, SPS and RHIC is shown by the dashed line in Fig. 1b, and has the fit function:

$$f_{AA}^L = -0.33 + 0.75 \ln(\sqrt{s_{NN}}) \quad (2)$$

With this fit equation, we extrapolated the scaled particle density per nucleon participant pair at the mid-rapidity region to LHC energy, $\sqrt{s_{NN}} = 5.5$ TeV:

$$\frac{1}{\langle N_{part}/2 \rangle} \times \frac{dN_{ch}}{d\eta}(\text{Pb} + \text{Pb at 5.5 TeV}) = 6.1$$

For $\langle N_{part} \rangle = 365.5$ obtained via the Glauber model calculation (using $\sigma_{NN} = 64$ mb) for 6% central Pb + Pb collisions at 5.5 TeV, this yielded:

$$\frac{dN_{ch}}{d\eta}(\text{central : 0 - 6\%, Pb} + \text{Pb at 5.5 TeV}) = 1120$$

The prediction of the Color Glass Condensate model (CGC model) [12] for $dN_{ch}/d\eta|_{|\eta|<1}/\langle N_{part}/2 \rangle$ in Pb + Pb collisions at LHC energy, $\sqrt{s_{NN}} = 5.5$ TeV, agrees very well with the results of extrapolation obtained with the logarithmic quadratic fit, as shown in Fig. 1b.

Fig. 2 plots the measured $dN_{ch}/d\eta$ of primary charged particles over a broad range of pseudorapidity, $|\eta| < 5.4$,

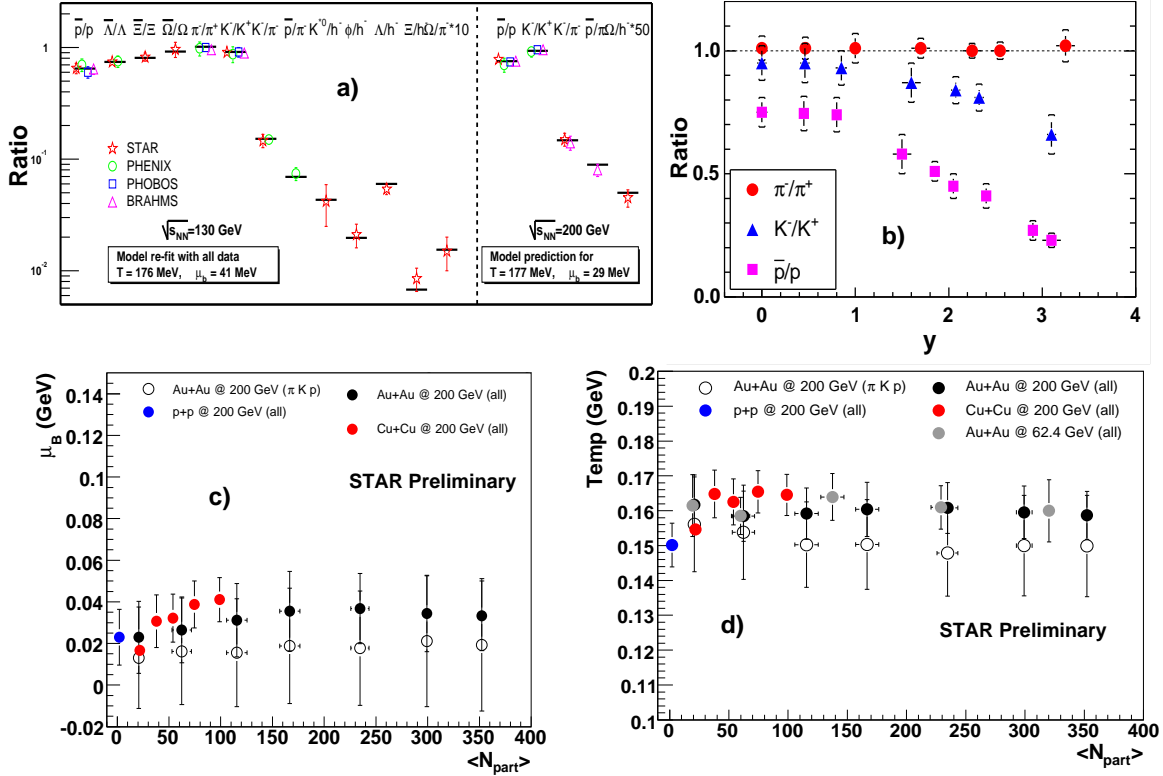


Fig. 3. Panel a) compares the experimental data from different particle multiplicity ratios obtained in Au + Au collisions at RHIC energies at $\sqrt{s_{NN}} = 130$ and 200 GeV with calculations from the thermal model [19]. Panel b) shows the ratios of antiparticles to particles as a function of rapidity [20]. The errors bars depict the statistical errors and the caps indicate the combined statistical errors. Panels c) and d), respectively, illustrate the thermal model fit baryon chemical potential (μ_B) and the temperature chemical freeze-out (T_{ch}) as function of collisions centrality ($\langle N_{part} \rangle$) [21]. μ_B and T_{ch} are obtained from Au + Au, Cu + Cu and p + p collisions at RHIC energies and for different particle species.

for Au + Au [8,9] and Cu + Cu [10,11] collisions under a variety of collision centralities and RHIC energies. The d + Au [13,14,15] and p + p [13] data at RHIC energies also are shown. The Cu + Cu, Au + Au d + Au and p + p data at all energies were obtained with the same detector setup in the PHOBOS experiment [16]. This is optimal because common systematic errors cancel each other out in the ratio. With this configuration, we were able to examine comprehensively particle production in Cu + Cu and Au + Au collisions for the same number of nucleon participant pairs, for the same fraction of total inelastic cross sections, and for the same geometry in both systems [11]. Both the height and width of the $dN_{ch}/d\eta$ distributions increase as a function of energy in both systems. Comparing the results revealed an interesting feature, namely that the best agreement of $dN_{ch}/\langle N_{part}/2 \rangle$ distributions over the full coverage, $|\eta| < 5.4$, for central and for peripheral Cu + Cu and Au + Au collisions is obtained for centrality bins selected to yield a similar geometry, i.e., a comparable value of $N_{part}/2A$ (where A is the atomic number) in both systems [11].

One question to be asked is whether mechanisms in the limiting fragmentation region (i.e. high $|\eta|$) are distinct from those at mid-rapidity ($|\eta| < 1$). From the results

shown in Fig. 2 for Au + Au, Cu + Cu, d + Au, and p + p collisions, there is no obvious evidence for two separate regions at any of the RHIC energies [10]. However, to date no such anomalies have been noted, at the AGS, SPS, or RHIC. So far, all results on particle pseudorapidity densities point to a rather smooth evolution in centrality and $\sqrt{s_{NN}}$. This of course, does not necessarily imply the absence of a phase transition, but rather, might indicate the insensitivity of these observables to the early phase of the collision and/or might suggest a second order phase transition (or a cross-over) [17]. We note that charged-particle production mechanisms for $dN_{ch}/d\eta$ shown in Fig. 2 are mostly obtained from the “soft” processes (see Fig. 1a).

2.2 Particle ratios and chemical freeze-out conditions

The chemical freeze-out point is the stage in the evolution of the hadronic system when inelastic collisions cease and the relative particle ratios become fixed; this point, is defined by the temperature chemical freeze-out, T_{ch} , and also by the baryon chemical potential, μ_B . These parameters, T_{ch} , and μ_B determine the particle composition of the hadronic final state. After chemical freeze-out, the particle composition inside the fireball is fixed, but elastic

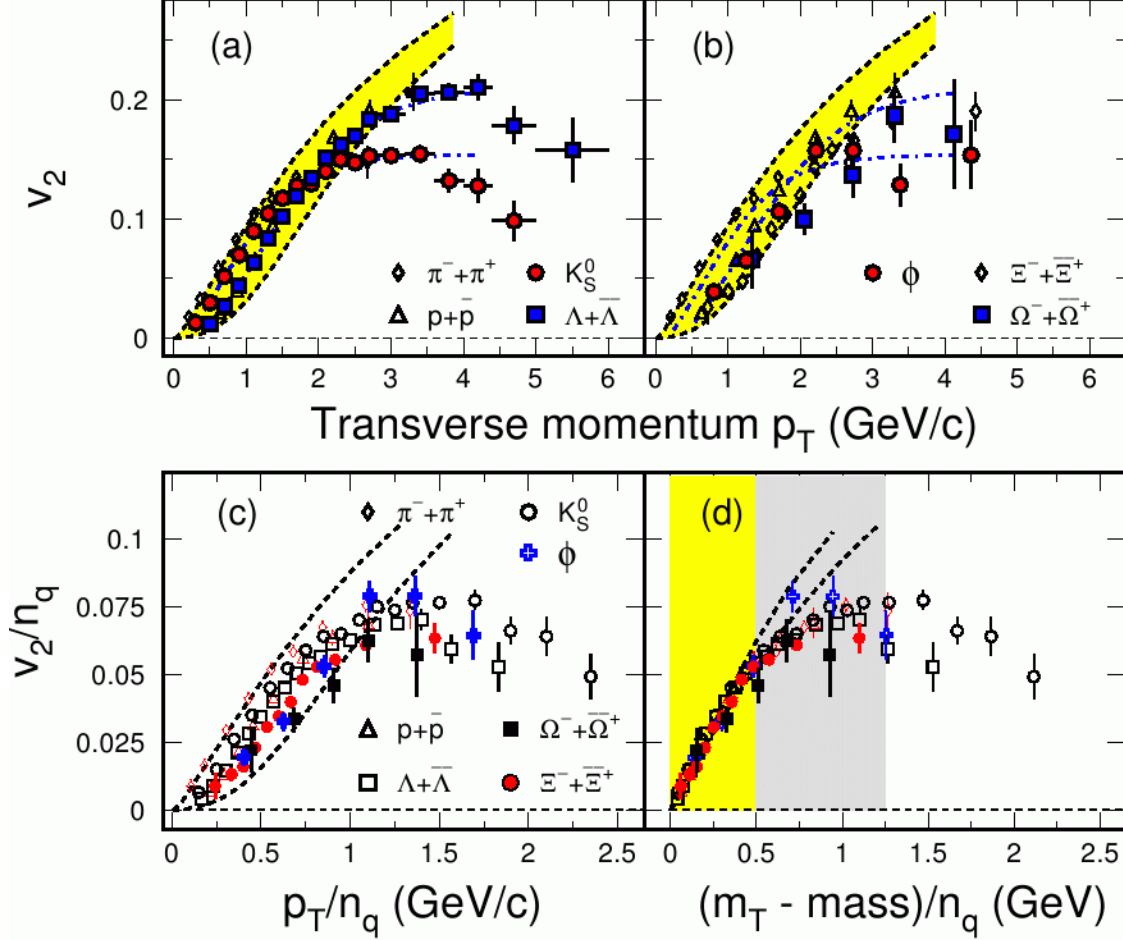


Fig. 4. Identified hadron anisotropy: Panels a) and b) as a function of transverse momentum p_T , panel c) as a function of scaled p_T/n_q and, panel d) as a function of scaled transverse kinetic energy $(m_T - \text{mass})/n_q$. n_q is the number of quarks in a given hadron (for mesons, $n_q = 2$; and, for baryons: $n_q = 3$). All data are from minimum-biased Au + Au collisions at $\sqrt{s_{NN}} = 200$ GeV [24].

collisions keep the system intact until the final, thermal freeze-out. At this stage the momentum distributions of particles are final and no longer change. Therefore, the transverse momentum spectra determine the parameters of the thermal freeze-out. Thereafter, statistical interpretation of particle production becomes an appropriate approach for evaluating heavy-ion collisions at high energies; because large multiplicities of hadrons are created. We can assume that the nuclear matter created in these collisions form an ideal gas that can be characterized by a grand-canonical ensemble. Using thermodynamic concepts to describe multiparticles production has a long history [18]. The concept of a temperature applies only to systems in at least local thermal equilibrium. The assumption of a locally thermalized source in chemical equilibrium can be tested by applying statistical thermal models to describe the ratios of various emitted particles.

Figure 3a compares the RHIC’s experimental particle ratios and statistical thermal model calculations for Au + Au collisions at 130 and 200 GeV [19]; note that the measurements were taken in the mid-rapidity region

$|\eta| < 1$. They demonstrate quantitatively the high degree of equilibration achieved for hadron production in central Au+Au collisions at RHIC energies. Values were obtained for (T_{ch}, μ_B) of $(174 \pm 7, 46 \pm 5)$ and $(177 \pm 7, 29 \pm 6)$ at 130 and 200 GeV, respectively. The model matches well with these results, and there is no indication of a significant change in T_{ch} at the two energies, 130 and 200 GeV. There is a drop in μ_B from ~ 46 MeV, at $\sqrt{s_{NN}} = 130$ GeV to 29 MeV at $\sqrt{s_{NN}} = 200$ GeV. We note that ratios involving multi-strange baryons are well reproduced, as is the ϕ/h^- ratio. Even relatively wide resonances such as the K^* ’s fit well with the picture of a chemical freeze-out.

The BRAHMS collaboration reported interesting results on particle ratios as a function of rapidity [20]. Figure 3b shows the π^-/π^+ , K^-/K^+ and \bar{p}/p ratios as a function of this parameter. We observe that the π^-/π^+ ratio is consistent with unity over the considered rapidity range, while the K^-/K^+ ratios drops almost by 30% at $y = 3$ from its mid-rapidity value, and the \bar{p}/p ratio by almost 70%. Fig. 3d and c show thermal model fit temperature and baryon potential at chemical freeze-out as a func-

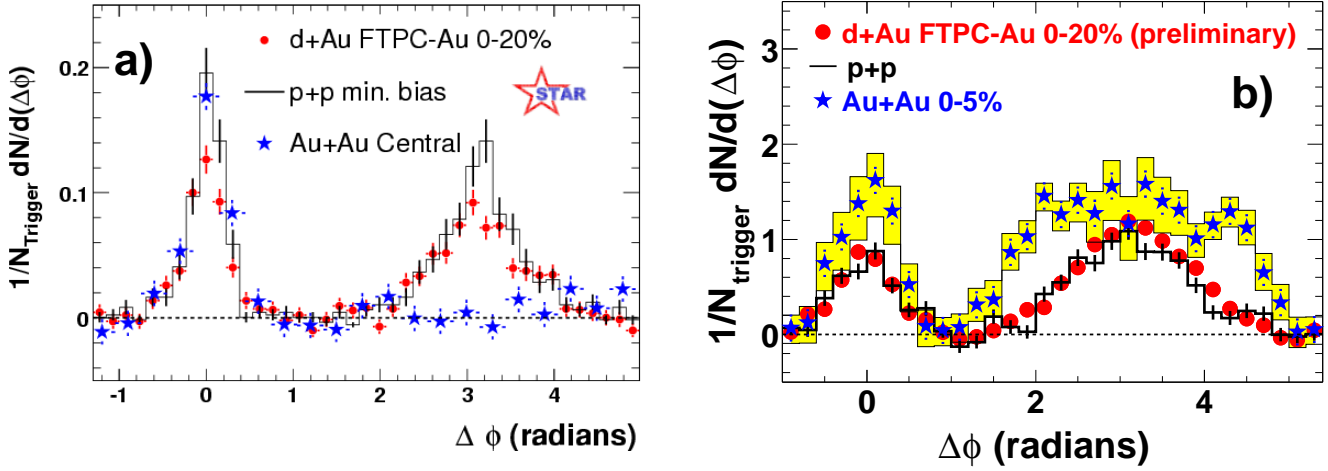


Fig. 5. Measurements of two-particle angular correlations in Au + Au, d + Au and p + p collisions at $\sqrt{s_{NN}} = 200$ GeV in the presence of a trigger particle with $p_T^{(t)}$ under the condition $4 < p_T^{(t)} < 6$ GeV/c, and an associated particle with $p_T^{(a)}$: panel a) for $2 < p_T^{(a)} < p_T^{(t)}$ GeV/c, and panel b) for $0.15 < p_T^{(a)} < 2$ GeV/c. The non-correlated background and the flow background were subtracted [30].

tion of collision centrality ($\langle N_{part} \rangle$) in Au + Au, Cu + Cu and p + p collisions at $\sqrt{s_{NN}} = 200$ GeV [21]. Temperature seems constant as a function of $\langle N_{part} \rangle$ and apparently independent of system size (Au + Au and Cu + Cu systems). The baryon chemical potential exhibits small variations as a function of N_{part} , consistent with of being independent of system size in Au + Au and Cu + Cu collisions.

3 Evidence of partonic matter at RHIC

3.1 Anisotropic flow of hadrons

The anisotropic flow of hadrons has been studied extensively in nucleus-nucleus collisions at the SPS and RHIC as a function of pseudorapidity, centrality, transverse momentum and energy [6, 22, 29]. In non-central collisions of heavy ions at high energy, the configuration space anisotropy is converted into a momentum space anisotropy. The dynamics of the collision determine the degree of this transformation. For a symmetric system, like Au + Au, the second Fourier expansion is a good parameterization of the anisotropy. At RHIC, a strong anisotropic flow (v_2) was observed for all hadrons measured suggesting that a strongly interacting system was created in the collisions.

Hydrodynamic models that assume the formation of a QGP were used to model the behavior of the medium so created [23]. Comparison of the data obtained at mid-rapidity region presented by the STAR, PHOBOS, and PHENIX collaborations [6, 29] to the hydrodynamic model [23] affords strong evidence that the originated medium behaves as a near ideal fluid.

Fig. 4 shows the anisotropic flow distributions, v_2 , for identified hadrons π , K_S^0 , p, Λ , Ξ , Ω and ϕ [24]. Calculations from a hydrodynamic model are depicted in dashed

lines, while the dot-dashed lines represent the results of fit for quark number scaling n_q (for mesons, $n_q = 2$; and, for baryons: $n_q = 3$). In the lower p_T region, $p_T \leq 2$ GeV/c, the value of v_2 is inversely related to the mass of the hadron, that is, characteristic of hydrodynamic collective motion in operation, see Fig 4a and b. At the intermediate p_T -region, the dependence is different. Instead of a mass dependence, there seems to be a hadron type dependence, Fig. 4(b). An interesting result concerns the ϕ meson, whose mass is close to that of p and Λ . The v_2 distribution illustrated as circles in Fig. 4b, is the same as the v_2 for π and Ω . It is known that the ϕ meson does not participate as strongly as others do in hadronic interactions, nor can ϕ mesons be formed via the coalescence-like $K^+ + K^-$ process in high energy collisions [25]. Hence, the strong v_2 we recorded must have developed before hadronization. This observation, together with the Ω v_2 results offer clear evidence for partonic collectivity [26]. To demonstrate the scaling properties of v_2 , the following transformation have been performed. The measured v_2 was scaled by the number of valence quarks in a given hadron. For mesons and baryons, respectively, they are $n_q = 2$ and 3. The p_T also was scaled with the same n_q . The results are shown in Fig. 4c. To include the effect of the collective motion, the p_T was transferred to the transverse kinetic energy $KE_T \equiv m_T - \text{mass} = \sqrt{p_T^2 - m^2} - m$ scaled by n_q , where m mass of the particle. The outcome is depicted in Fig. 4d. All of the hadron v_2 scaled nicely up to $(m_T - \text{mass})/n_q \sim 1.2$. Hydrodynamic calculations [27], shown as dashed-lines in the plot, also are scaled in the low p_T -region. At high- p_T , the values of v_2 appear to fall. These observations about scaling reveal that before hadronization, quarks already have acquired the collective motion v_2 , and that when they coalesce, the v_2 is passed

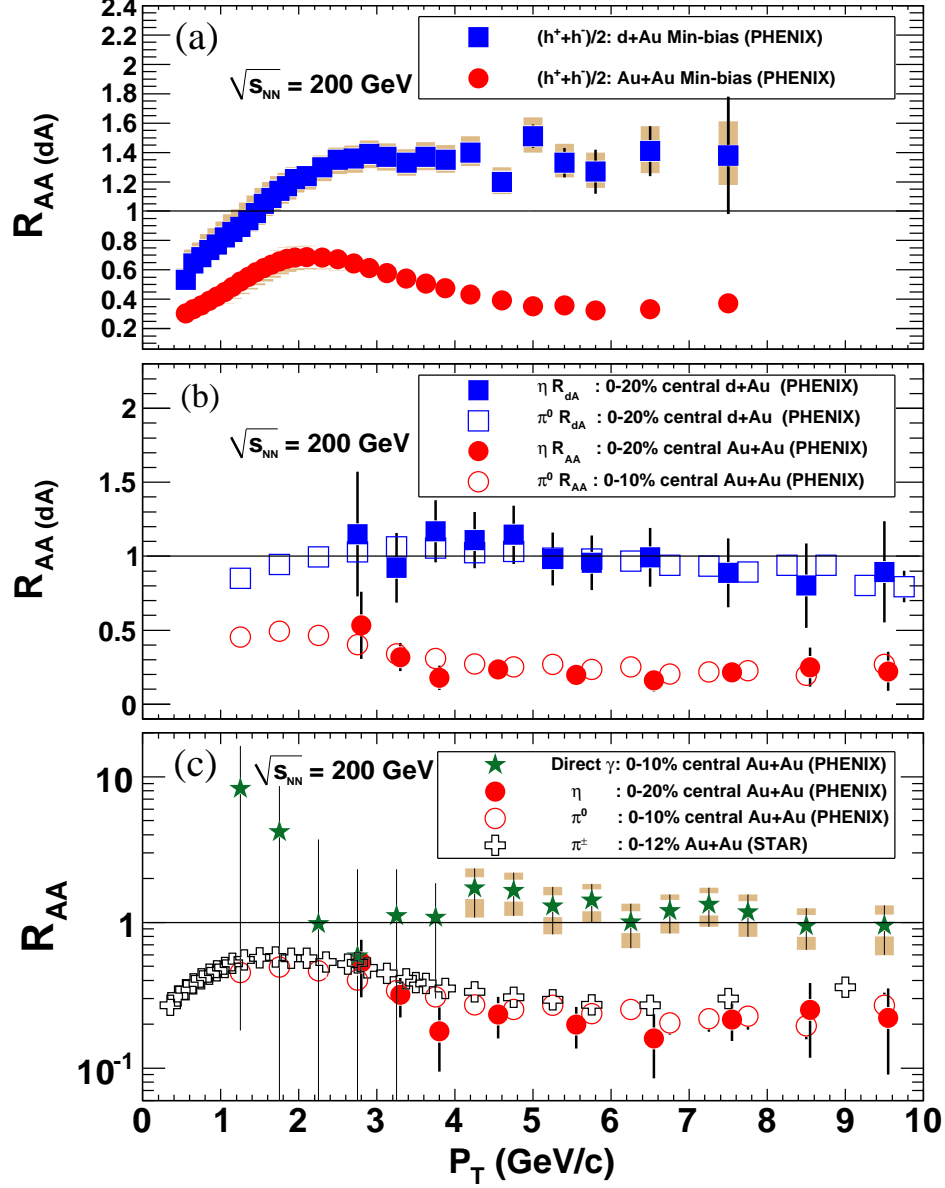


Fig. 6. Compilation of data of nuclear modification factor R_{AA} from Au + Au collisions and R_{dA} of d + Au collisions at $\sqrt{s_{NN}} = 200$ GeV using Refs. [34]. Panel a) compares R_{AA} with R_{dA} for charged hadrons, $(h^+ + h^-)/2$, from minimum bias Au + Au and d + Au collisions. Panel b) compares R_{AA} with R_{dA} for π^0 and η from central Au + Au and d + Au collisions. Panel c) compares the R_{AA} of Direct γ with R_{AA} of π^0 , η and π^\pm in central Au + Au collisions. The error bars correspond to the statistical errors. For clarity, the systematic errors are shown as vertical bands.

to newly formed hadrons. Again this observation verifies partonic collectivity.

4 Signatures of dense matter at RHIC

4.1 Di-jet fragment azimuthal correlations

The study of high transverse momentum hadron production in heavy ion collisions at RHIC provides an experimental probe of the QCD matter in the most dense stage of the collisions, wherein quark-gluon deconfinement is

likely to occur [28]. In particular, two-hadron azimuthal correlations support the assessment of back-to-back, hard-scattered partons that propagate in the medium before fragmenting into jets of hadrons, thereby serving as a tomography probe of the medium.

Fig. 5 shows measurements of two-particle correlations [30] given a trigger particle $p_T^{(t)}$ under the condition $4 < p_T^{(t)} < 6$ GeV/c, along with an associated particle with $p_T^{(a)}$: 1) for $2 < p_T^{(a)} < p_T^{(t)}$ GeV/c as shown in Fig. 5a, and 2) for $0.15 < p_T^{(a)} < 2$ GeV/c as shown in Fig. 5b. The two-particle correlation are presented as a function of the dif-

ference between the azimuthal angles of the two particles ($\Delta\phi$) produced in Au + Au, d + Au and p + p collisions at $\sqrt{s_{NN}} = 200$ GeV. These measurements were made at the mid-rapidity region $0 < |\Delta\eta| < 1.4$

Fig. 5a demonstrates that the trigger-side correlation peak in central Au + Au collisions apparently is the same as that measured in p + p and d + Au collisions but the away-side jet correlation in Au + Au has vanished. This observation is consistent with a large energy loss in the medium causing it to be opaque to the propagation of high momentum partons. However, it is noticeable in Fig. 5b, which has a wide $p_T^{(a)}$, $0.15 < p_T^{(a)} < 2$ GeV/c, that the away side jets have not really disappear, but simply lost energy so that the away-side correlation peak has become much wider than that of the p + p and d + Au collisions. These collective measurements, from p + p, d + Au and Au + Au of two-particle correlations, point to the creation of a dense medium in central Au + Au collisions at $\sqrt{s_{NN}} = 200$ GeV.

4.2 High- p_T hadron suppression: jet-suppression

In heavy ion collisions (from AGS to RHIC energies) hadron production at the mid-rapidity region ($|y| < 1.5$) rises with increasing collision energy. At RHIC, the central zone is almost baryon free [31]. Particle production is large and dominated by pair production, and the energy density seems to exceed significantly that required for QGP formation [6].

Recently, RHIC experiments revealed suppression of the high transverse momentum component, p_T of hadron spectra at the mid-rapidity region in central Au+Au collisions compared to scaled momentum spectra from p+p collisions at the same energy, $\sqrt{s_{NN}} = 200$ GeV [6]. This effect, originally proposed by Bjorken, Gyulassy and others [32] rests on the expectation of a large energy loss of high momentum partons scattered in the initial stages of collisions in a medium with a high density of free color charges. According to QCD theory, colored objects may lose energy by the bremsstrahlung radiation of gluons [33]. Such a mechanism would strongly degrade the energy of leading partons, reflected in the reduced transverse momentum of leading particles in the jets emerging after fragmentation into hadrons. The STAR experiment established that the topology of high- p_T hadron emission is consistent with jet emission, so that jet-suppression is a valid concept.

Fig. 6 shows compilation of data using Refs. [34] for the nuclear modification factors measured for different collisions systems at RHIC energies. The nuclear modification factor is defined as:

$$R_{AA}(p_T) = \frac{\text{yield per A + A collisions}}{N_{bin} \times (\text{yield per p + p collisions})} \\ = \frac{d^2N^{A+A}/dp_T d\eta}{N_{bin} d^2N^{p+p}/dp_T d\eta}$$

It involves scaling measured distributions of nucleon-nucleon transverse momentum by the number of expected incoherent binary collisions, N_{bin} [35]. In the absence of any modifications due to the ‘embedding’ of elementary collisions

in a nuclear collision, we expect $R_{AA} = 1$ at high- p_T . At low p_T , where particle production follows a scaling with the number of participants, the above definition of R_{AA} leads to $R_{AA} < 1$ for $p_T < 2$ GeV/c.

In d + Au collisions at RHIC energy ($\sqrt{s_{NN}} = 200$ GeV) as shown in Fig. 6a, the R_{dA} for charged hadrons ($h^+ + h^-$)/2 is enhanced. This enhancement was expected as a consequence of Cronin enhancements, now understood as an initial state effect [36] which also is seen in pA collisions. The Cronin effect is associated with the initial multiple scattering of high momentum partons. In contrast, RHIC experiments discovered a factor of 4-5 suppression, in central Au + Au (at $\sqrt{s_{NN}} = 200$ GeV). In the same context, the R_{dAu} of π^0 and η in central d + Au collisions exhibits no suppression of high- p_T , in contrast with the R_{AA} of π^0 and η in central Au + Au collisions that is suppressed, as shown in Fig. 6b. At $p_T \sim 4$ GeV/c, we find a ratio $R_{dAu}/R_{AA} \approx 5$. Indeed, the R_{dA} distribution shows the Cronin type enhancement observed at lower energies as in Pb + Pb collisions at 17.3 GeV/c [37].

Fig. 6c summarizes the present status of R_{AA} for direct photons, π^0 and η in central Au + Au collisions at $\sqrt{s_{NN}} = 200$ GeV. The R_{AA} for direct photons are not suppressed because they do not interact strongly with the medium. The R_{AA} for both π^0 and η ’s mesons exhibit the same suppression relative to the point-like scaled p + p data by a factor of ~ 5 which appears to be constant for $p_T > 4$ GeV/c while the η mass is much larger than that of π^0 . This observation combined with Fig. 4 is clearly an indication of partonic nature of suppression.

This data of R_{AA} were described by theoretical calculations of parton energy loss in the matter created in Au+Au collisions [38]. From these theoretical frameworks, we have learned that the gluon density dN_g/dy must be approximately 1000 [39], and the energy density of the matter created in the most central collisions must be approximately 15 GeV/fm³ to account for the large suppression observed in the data [40].

5 Heavy-flavors as probes for dense medium

As discussed above, RHIC has produced in high-energy central Au + Au collisions at $\sqrt{s_{NN}} = 200$ GeV a new form of matter that is dense, strongly interacting and can be partonic, called sQGP. This new state of strongly interacting matter can closely resemble a “perfect” fluid, with very low viscosity and high opacity explained by the equations of hydrodynamics [23]. The research focus now has shifted from this initial discovery to a detailed exploration of partonic matter. Particles carrying a heavy flavor, i.e., charm or beauty quarks, are powerful tool for studying the properties of the hot, dense medium created in high-energy nuclear collisions: they are generated early in the reaction, and subsequently diffuse in the putative sQGP.

The study of heavy flavor in relativistic nuclear collisions follows two different approaches: 1) The direct reconstruction of the heavy flavor meson, and 2) the identification of electrons and muons from semi-leptonic de-

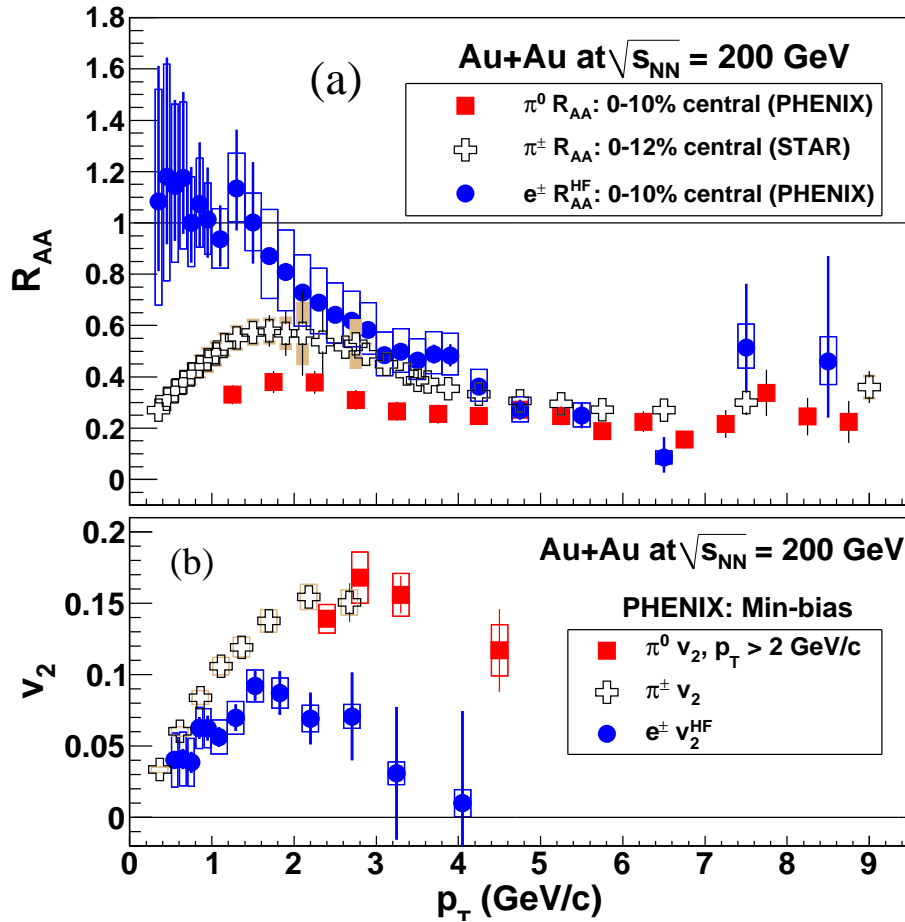


Fig. 7. Compilation of data on Au + Au collisions at $\sqrt{s_{NN}} = 200$ GeV from Refs. [34,41]. Panel a) represents the nuclear modification factor of heavy-flavor electrons R_{AA}^{HF} compared with the R_{AA} of π^0 and π^\pm in central Au + Au collisions. Panel b) considers the anisotropic flow of heavy-flavor electrons v_2^{HF} with that of v_2 of π^0 and π^\pm in minimum-bias Au + Au collisions $\sqrt{s_{NN}} = 200$ GeV. The error bars correspond to the statistical errors. For clarity, the systematic errors are shown as vertical boxes and bands.

cays of such mesons. The PHENIX and STAR experiments at RHIC explore one or both of these methods. The STAR collaboration is directly reconstructing heavy flavor mesons the decay channel $D^0 \rightarrow K^- + \pi^+$ in d + Au and Au + Au collisions. Employing semi-leptonic decays of heavy flavor mesons, such as $D^0 \rightarrow e^+ + K^+ + \nu$ over a broad p_T range, more efficiently measures charm and bottom quark production and overcomes the limitation imposed by directly reconstructing such mesons.

At RHIC, two methods are utilized to measure heavy flavor production via semi-leptonic decays: 1) Identification of electrons from the decays of D and B -mesons, and 2) identification of muons from D -meson decays. The PHENIX and STAR experiments pursue the analysis of non-photonic electrons (from heavy flavor) [41,42]. Electron identification in PHENIX largely is based on using the Ring Imaging Cherenkov detector (RICH) in conjunction with a highly granular EMC (electromagnetic calorimeter). Their momentum is derived from the curvature of the track (due to a magnetic field up to 1.15 Tesla) reconstructed from drift and pad chambers. STAR

identifies electrons using information on dE/dx and momentum gleaned from the Time Projection Chamber (TPC) and the Time of Flight (ToF) data for the low to moderate p_T ($p_T < 4-5$ GeV/c) electrons. The barrel electromagnetic calorimeter’s (EMCAL’s) data is used for moderate to high- p_T ($p_T > 1.5$ GeV/c) electrons [42]. A major difficulty in both collaborations’ electron analyses is the fact that there are many sources of electrons other than the semi-leptonic decays of heavy flavor mesons. The main sources of background are photon conversion in the detector material (less significant in PHENIX that has a lesser amount of material than STAR), and π^0 and η Dalitz decays. Other sources of background such as ω , ϕ and ρ decays also must be taken into account. The background sources usually are called photonic electrons.

Fig. 7 shows compilation of data using Refs. [34,41,42] of the nuclear modification factors and elliptic flow measured for Au + Au collisions systems at $\sqrt{s_{NN}} = 200$ GeV. Fig. 7a compares the nuclear modification factor R_{AA} of heavy flavor electrons to π^0 data, and to π^\pm data obtained from central Au + Au collisions at $\sqrt{s_{NN}} = 200$ GeV. We

observe clear suppression of heavy flavor electrons in central events in high- p_T . For $p_T > 4$ GeV/c, the R_{AA} of heavy flavors is surprisingly similar to that for π^0 and π^\pm . Fig. 7b illustrates the distribution of the anisotropy of heavy flavors electrons (v_2^{HF}) as a function of the particles’ transverse momentum, p_T , in minimum bias Au + Au collisions at $\sqrt{s_{NN}} = 200$ GeV. Collective behavior is apparent in heavy-flavor electrons ($v_2^{HF} > 0$); but however, it is lower than v_2 of π^0 for $p_T > 2$ GeV/c.

This data presented in Fig 7 indicates that heavy flavors strongly coupled with the medium. The observed suppression at high- $p_T > 4$ GeV/c can be explained in terms energy loss from the heavy-flavors into the medium. Ref. [41] offers different theoretical predictions for heavy-flavor electrons in central Au + Au collisions, considering different energy loss mechanisms. However, I note that in Fig. 7b, the data extend only to around $p_T \approx 4$ GeV/c, and there are large statistical errors in the v_2^{HF} . This implies that we can reach a comprehensive conclusion about R_{AA}^{HF} and v_2^{HF} only when we have more data on Au + Au collisions at $\sqrt{s_{NN}} = 200$ GeV is needed and an upgrade of PHENIX and STAR detectors is required. Furthermore, we need measurements of the particles identified as decay products from charm or beauty flavors using the displacement of their trajectories from the collision vertex (measuring the distance of closest approach, DCA). Fortunately, both detectors PHENIX and STAR already were upgrade by building silicon vertex trackers for heavy flavors [43, 44].

6 Conclusions

I discussed measurements from RHIC collisions on bulk particle production, the initial conditions of the collisions, particle ratios and chemical freeze-out conditions, flow anisotropy of particles, di-jet fragment azimuthal correlations, high- p_t hadron suppression and heavy-flavors probes as a function of collision centrality, energy, system sizes and for different particle species. The measurements suggest that RHIC discovered a new state of matter in central Au + Au collisions at $\sqrt{s_{NN}} = 200$ GeV. This new form of matter is a hot, dense, strongly interacting and is called “sQGP”. Whilst this material, and its discovery, is far being fully understood, the focus of the RHIC experiments has shifted from the discovery phase to a detailed exploration phase of the properties of the medium. The hope is that Pb + Pb collisions at LHC energies (LHC energy is approximately 30 times higher than RHIC’s maximum energy: $LHC\text{-energy}/RHIC\text{-energy} = 5500/200 = 27.5$) will create a medium with an initial temperature high enough so that the interaction weakens sufficiently to generate a gaseous QGP.

Acknowledgements

The author’s research was supported by US Department of Energy, DE-AC02-98CH10886. The author would like to thank the organizers for an enjoyable and stimulating workshop. Special thanks to Mark Baker and Nu Xu for a careful reading of

the manuscript and useful suggestions, and Ralf Averbeck for providing PHENIX data plotted on figure 7.

References

1. S. Shuryak, Phys. Rep. **61**, (1980) 71; L. McLerran, Rev. Mod. Phys. **58**, (1986) 1021.
2. H. Satz, Nucl. Phys. A **715** (2003) 3c.
3. F. Karsch, Nucl. Phys. A **698** (2002) 199c.
4. J. Hofman, *et al.*, in Bear Mountain Workshop, New York, December 19974; H.G. Baumgardt, *et al.*, Z. Phys. A **273** (1975) 359.
5. <http://www.agsrhichome.bnl.gov/RHIC/Runs/>
6. I. Arsene *et al.* Nucl. Phys. A **757** (2005) 1; B. B. Back *et al.* Nucl. Phys. A **757** (2005) 28; J. Adams *et al.* Nucl. Phys. A **757** (2005) 102; K. Adcox *et al.* Nucl. Phys. A **757** (2005) 184.
7. R. Nouicer *et al.*, Eur. Phys. J. C **33** (2004) S606.
8. R. Nouicer *et al.*, The GIOI publishers : 2002 QCD and Hadronic Interactions, edited by Tran Thanh Van, (2002) 381.
9. B.B. Back *et al.* Phys. Rev. Lett. **91**, (2003) 502303.
10. R. Nouicer *et al.* AIP Conf. Proc. 842 (2006) 86; R. Nouicer e-Print: e-Print arXiv-nucl-ex/0601026;
11. B. Alver *et al.* e-Print: arXiv:0709.4008 (submitted to Phys. Rev. Lett. (2007)).
12. D. Kharzeev *et al.* Nucl. Phys. A **747** (2005) 609; e-Print arXiv:hep-ph/0408050.
13. R. Nouicer *et al.* J. Phys. G **30**, (2004) S113.
14. B.B. Back *et al.* Phys. Rev. Lett. **93**, (2004) 082301.
15. B.B. Back *et al.* Phys. Rev. C **72**, (2005) 031901(R).
16. R. Nouicer *et al.* Nucl. Instrum. Meth. in Physics Research A **461**, (2001) 143; B.B. Back *et al.* Nucl. Instrum. Meth. in Physics Research A **499**, (2003) 603.
17. T.S. Ullrich Eur. Phys. J. **A 19** (2004) s01.
18. R. Hagedorn Supl. A. Nuovo Cimento Vol III **No.2** (1965) 150.
19. P. Braun-Munzinger *et al.* Phys. Lett. B **518** (2001) 41; e-Print arXiv-nucl-th/0304013
20. I. G. Bearden *et al.* Phys. Rev. Lett. **90**, (2003) 102301.
21. J. Takahashi (for the STAR Collaboration), talk given at the International Conference on Strangeness in Quark Matter 2008 (SQM2008), October 6, 2008 at Beijing, China. J. Takahashi *et al.* e-Print arXiv[nucl-ex/0809.0823.
22. C. Alt *et al.* Phys. Rev. C **68** (2003) 034903; and references therein.
23. T. Hirano, Acta Phys. Polon. B **36** (2005) 187; U.W. Heinz e-Print arXiv-nucl-th/0512051.
24. B.I. Abelev *et al.* Phys. Rev. Lett. **99** (2007) 112301; e-Print arXiv-nucl-ex/0703033; N. Xu Braz. Jou. Phys. **37 2C** (2007) 773.
25. J. Adams *et al.* Phys. Lett. B **612**, 181 (2005) 181; S. Blyth *et al.* proceedings of International Conference on Strangeness in Quark Matter, Los Angeles, California, 26 - 31 March 2006; e-Print arXiv-nucl-ex/060801
26. J. Adams *et al.* Nucl. Phys. A **757** (2005) 102.
27. P. Huovinen *et al.* Phys. Lett. B **503** (2001) 58.
28. P. Jacobs *et al.*, Prog. Nucl. Phys. **54**, (2005) 443.
29. R. Nouicer *et al.* J. Phys. G **34** (2007) S887.
30. J. Adams *et al.* Phys. Rev. Lett. **91** (2003) 072304; J. Adams *et al.* Phys. Rev. Lett. **95** (2005) 152301; M.J. Tannenbaum PoS (CFRNC 2006) 001.

31. I.G. Bearden *et al.* Phys. Rev. Lett. **93** (2004) 102301;
 32. J.D. Bjorken, Phys. Rev. D **27** (1983) 140; X.N. Wang *et al.* Phys. Rev. Lett. **68** (1992) 1480; and M. Gyulassy *et al.* Phys. Lett. B **243** (1990) 432.
 33. J.J. Gaardhøje *et al.* Nucl. Phys. A **734** (2004) 13.
 34. B.I. Abelev *et al.* Phys. Lett. B **655** (2007) 104; S.S. Adler *et al.* Phys. Rev. Lett. **98** (2007) 172302; S.S. Adler *et al.* Phys. Rev. Lett. **96** (2006) 202301; S.S. Adler *et al.* Phys. Rev. Lett. **91** (2003) 072303.
 35. C. Albajar *et al.* Nucl. Phys. B **355** (1990) 261; J. Adams *et al.* Phys. Rev. Lett. **91** (2003) 172302.
 36. A. Accardi Contribution to the CERN Yellow report on Hard Probes in Heavy Ion Collisions at the LHC (2002); e-Print: arXiv:hep-ph/0212148.
 37. M. Gyulassy *et al.* Nucl. Phys. A **750** (2005) 30.
 38. I. Vitev *et al.* Nucl. Phys. A **715** (2003) 779; X.-N. Wang, Phys. Lett. B **595** (2004) 165; X.-N. Wang, Phys. Lett. B **579** (2004) 299; C.A. Salgado *et al.* Phys. Rev. D **68** (2003) 014008.
 39. I. Vitev *et al.* Phys. Rev. Lett. **89** (2002) 252301.
 40. I. Vitev, J. Phys. G **30** (2004) S791.
 41. S.S. Alder *et al.* Phys. Rev. Lett. **98** (2007) 17230; S.S. Alder *et al.* Phys. Rev. Lett. **96** (2006) 032001; S.S. Alder *et al.* Phys. Rev. Lett. **96** (2006) 032301;
 42. J. Adams *et al.* Phys. Rev. Lett. **94** (2005) 062301; A.A.P. Suaide Braz. Jour. of Phys. **37** (2007) 2c.
 43. M. Baker *et al.*, Proposal for a Silicon Vertex Tracker (VTX) for the PHENIX Experiment, BNL- 72204-2004, Physics Dept. BNL (2004). R. Nouicer *et al.* Nuclear Instruments and Methods in Physics Research B **261** (2007) 1067; R. Nouicer *et al.*, POS VERTEX2007 (2007) 042.
 44. C. Chasman *et al.* LBNL **5509** (2008).

Table 1. RHIC operating modes and total integrated luminosity delivered to all experiments for each run [5].

Run	Species	Total particle energy: $\sqrt{s_{NN}}$ [GeV/nucleon]	Total delivered luminosity	Average Store polarization
Run 1	Au+Au	55.8	$< 0.001 \mu\text{b}^{-1}$	-
	Au+Au	130.4	$< 20 \mu\text{b}^{-1}$	-
Run 2	Au+Au	200.0	$< 258 \mu\text{b}^{-1}$	-
	Au+Au	19.6	$< 0.4 \mu\text{b}^{-1}$	-
	pol. p+p	200.0	$< 1.4 \text{pb}^{-1}$	15%
Run 3	d+Au	200.0	73nb^{-1}	-
	pol. p+p	200.0	$< 5.5 \text{pb}^{-1}$	34%
Run 4	Au+Au	200.0	$3530 \mu\text{b}^{-1}$	-
	Au+Au	62.4	$67 \mu\text{b}^{-1}$	-
	pol. p+p	200.0	7.1pb^{-1}	46%
Run 5	Cu+Cu	200.0	42.1nb^{-1}	-
	Cu+Cu	62.4	1.5nb^{-1}	-
	Cu+Cu	22.4	0.02nb^{-1}	-
	pol. p+p	200.0	29.5pb^{-1}	46%
Run 6	pol. p+p	200.0	88.6pb^{-1}	58%
	pol. p+p	62.4	$< 1.05 \text{pb}^{-1}$	50%
Run 7	Au+Au	200.0	$7250 \mu\text{b}^{-1}$	-
	Au+Au	9.2	test only	-
Run 8	d+Au	200.0	437nb^{-1}	-
	pol. p+p	200.0	38.4pb^{-1}	45%
	Au+ Au	9.2	-	-